ARTICLE

Computational design of graphitic carbon nitride photocatalysts for water splitting

Gareth O. Hartley,[a,b] Natalia Martsinovich [a] *

A series of structures based on graphitic carbon nitride (g-C_3N_4), a layered material composed of linked carbon-nitrogen heterocycles arranged in a plane, were investigated by density functional theory calculations. g-C_3N_4 is a semiconductor that absorbs UV light and visible light at the blue end of the visible spectrum, and is widely studied as a photocatalyst for water splitting; however, its photocatalytic efficiency is limited by its poor light-harvesting ability and low charge mobilities. Modifications to the g-C_3N_4 structure could greatly improve its optical and electronic properties and its photocatalytic efficiency. In this work, the g-C_3N_4 structure was modified by replacing the nitrogen linker with heteroatoms (phosphorus, boron) or aromatic groups (benzene, s-triazine and substituted benzenes). Two-dimensional (2D) sheets and three-dimensional (3D) multilayer structures with different stacking types were modelled. Several new structures were predicted to have electronic properties superior to g-C_3N_4 for use as water splitting photocatalysts. In particular, introduction of phosphorus, benzene and s-triazine groups led to band gaps smaller than in the standard g-C_3N_4 (down to 2.4 eV, corresponding to green light). Doping with boron in the linker positions dramatically reduced the band gap (to 1.6 eV, corresponding to red light); the doped material has the valence band position suitable for water oxidation. Our computational study shows that chemical modification of g-C_3N_4 is a powerful method to tune this material's electronic properties and improve its photocatalytic activity.

1. Introduction

Graphitic (or polymeric) carbon nitride (g-C_3N_4) is a long known material, first reported in 1834 under the name "melon".[1] Although C_3N_4 has several allotropes including α-C_3N_4, β-C_3N_4, cubic-C_3N_4 and pseudocubic-C_3N_4, g-C_3N_4 is the most stable form.[2] It is an organic semiconductor composed of carbon and nitrogen in a layered structure made of graphene-like extended sheets with gentle layer undulations.[3] Graphitic carbon nitride has attracted increased attention during the last decade,[4-7] since the report in 2009 of its application as a visible light photocatalyst for hydrogen evolution from water.[8]

Photocatalytic hydrogen production is regarded as a very promising approach to generate clean fuels, as a possible replacement to fossil fuels which have well-known problems of carbon emissions, limited supply, high extraction costs and supply chain volatility.[9] Hydrogen as a fuel, in contrast, has the potential to be renewable (being generated from water) and produce clean emissions (it burns to produce water).[10-11] Photocatalytic water splitting would be an ideal means of hydrogen production, since it uses an abundant feedstock material (water) and is driven by a renewable energy source (solar energy). The process of photocatalytic water splitting is initiated via the absorption of a photon by a photocatalyst; this induces photoexcitation of electrons from the valence band to the conduction band, thereby generating an electron-hole pair (e^-/h^+). The electron and the hole are then able to participate in charge transfer processes with species that are adsorbed onto the photocatalyst surface, such that reduction and oxidation of the adsorbed species can be respectively stimulated. In the case of water splitting, transfer of the excited electron from the photocatalyst conduction band to water protons induces reduction of protons, forming molecular hydrogen. Similarly, transfer of photo-holes from the valence band to water species induces water oxidation. Thus a good photocatalyst should be able to absorb sunlight efficiently, and both its conduction band and valence band should be suitably positioned to allow transfer of photoexcited electrons and holes to the water species.[10, 12] A number photocatalysts for hydrogen evolution have been developed, primarily inorganic semiconductors, such as TiO_2 and other metal oxides.[10, 12]

Thus far, the efficiency of direct water splitting has been low for a number of reasons, such as the inefficient harvesting of visible light, recombination of photo-electrons with holes, and recombination of reaction intermediates to form water instead of H_2 and O_2.[10, 13] Approaches have been developed to minimise recombination, e.g. by using cocatalysts (noble metals such as Pt and Pd) to facilitate charge separation,[13] and

a. Department of Chemistry, University of Sheffield, Brook Hill, Sheffield, S3 7HF, United Kingdom.
b. Department of Materials, University of Oxford, Parks Road, Oxford, OX1 3PH, United Kingdom.

by adding organic sacrificial agents,[11, 14] which are easily oxidised by photo-holes and thus are effective at eliminating holes, leading to greatly diminished electron-hole recombination, so that excited electrons have longer lifetimes and have improved chances of participating in hydrogen reduction reactions.[11] However, the long-standing problem is the inefficient harvesting of visible light.[15] The majority of inorganic photocatalysts are predominantly active under ultraviolet irradiation. Few photocatalysts have been identified which satisfy both water reduction and oxidation potentials and which also possess band gap energies accessible to visible light.[11] Techniques such as dye sensitisation have enabled the light harvesting restrictions of wide band gap photocatalysts to be bypassed.[16] However, the realisation of narrow band gap water splitting photocatalysts remains highly desirable. Conventional methods of introducing dopants to form band gap states can improve light absorption, but this is often accompanied by increased rates of electron-hole recombination, which decreases photocatalyst efficiencies.[15]

g-C_3N_4 is in many ways an ideal material for photocatalytic applications. It is nontoxic and cheap to synthesise from urea, dicyandiamide or melamine by calcination.[5] The valence and conduction band energies of g-C_3N_4 are such that the material is a moderate bandgap (2.7 eV, blue light) semiconductor.[8] However, it remains inefficient as a photocatalyst, since only short wavelength visible light can stimulate this band gap transition. Moreover, in most experiments, g-C_3N_4 can facilitate only hydrogen evolution catalysis, with few examples of simultaneous evolution of oxygen and hydrogen being reported.[17-18]

However, one of the advantages of g-C_3N_4 is that its chemical nature as an organic polymer makes its structure amenable to modifications. This material is composed of tri-s-triazine (heptazine) units, connected by nitrogen linkers and forming two-dimensional (2D) layers;[3, 8] the layers are stacked in three dimensions (3D) in AB stacking, similar to graphite.[3] The idealised 2D lattice of fully polymerised nitrogen-linked heptazine units is shown in panel (1) of Figure 1. It has to be noted that this fully polymerised structure has not been confirmed experimentally; typically, experiments produce a partially polymerised structure, which still consists of nitrogen-linked heptazine units in 2D, but each nitrogen linker connects two rather than three heptazines.[3, 19] Heptazine or s-triazine and have been considered as the likely structural units; ab initio studies indicated that heptazine-based structures are thermodynamically favoured,[20] in agreement with later X-ray diffraction studies.[3, 19] However, triazine-based layered carbon nitride has been prepared as well.[21] Another related type of structure is a covalent triazine framework, where triazine units are connected by aromatic linkers, such as benzene or nitrogen heterocycles.[22-23]

Structural modifications were shown to improve the photocatalytic performance of g-C_3N_4.[5] The approaches can be classified into morphological modifications and chemical modifications. The morphology and thus physical properties of g-C_3N_4 can be controlled to an extent by the choice of synthesis. In particular, mesoporous graphitic carbon nitride (mpg-C_3N_4) with pores 2-50 nm in diameter has been produced by templating;[5, 24] its advantage for photocatalytic applications is the much larger surface area compared to bulk g-C_3N_4.[25] 2D nanosheets ca. 2 nm in thickness have been manufactured by such methods as thermal oxidation etching of bulk g-C_3N_4 in air,[26] exfoliation of bulk g-C_3N_4 in water,[27] and high-temperature H_2 treatment of bulk g-C_3N_4.[28] Quantum confinement results in band gaps of 2D carbon nitride nanosheets increasing by ~0.2 eV compared to the bulk material, which hampers visible light harvesting;[26, 28-29] however, at the same time it is reported to lead to improved electron transport and increased lifetimes of charge carriers;[26, 29] the surface area of nanosheets is increased compared to their bulk analogues, which is beneficial for photocatalysis. On balance of these factors, carbon nitride nanosheets often have improved photocatalytic activities.[28-29]

Chemical modification of g-C_3N_4 has also been achieved by in-situ or post-synthesis elemental doping with a host of elements, such as B,[30] C,[31] O,[32] F,[33] P,[34] S[35] and Cl.[36] Functionalisation of carbon nitride by attaching organic side groups, such as barbituric acid, has also been reported.[37] In all cases, doping was shown to improve the materials' photocatalytic activities.

This very brief overview shows that structural modification of graphitic carbon nitride is achievable and that both morphological modifications (e.g. nanosheets) and chemical modifications (doping) improve this material's photocatalytic efficiency. However, the majority of these experimental studies use the trial and error approach, focussing on efficiencies rather than on underlying mechanisms. Therefore theoretical studies are needed, to understand the mechanisms behind the improvements in these materials photocatalytic activities.

In this work, we take a systematic approach and design a series of new 2D frameworks based on g-C_3N_4, with the aim of identifying such modifications that would improve the material's light absorption properties and overall photocatalytic performance. Inspired by the reports of elemental doping of g-C_3N_4[30-37] and covalent triazine frameworks,[22-23] we replace the nitrogen linker in the g-C_3N_4 structure with heteroatoms (boron or phosphorus), and with organic species capable of three-fold coordination: s-triazine, benzene and substituted benzenes (Figure 1). For simplicity, we consider the fully condensed g-C_3N_4 as the basic structure. We consider the 3D stacking of these 2D structures and the effect of stacking on the electronic properties of these materials. We analyse the electronic properties (band gaps and band positions) of these candidate structures with emphasis on the suitability of these novel materials for water splitting.

ARTICLE
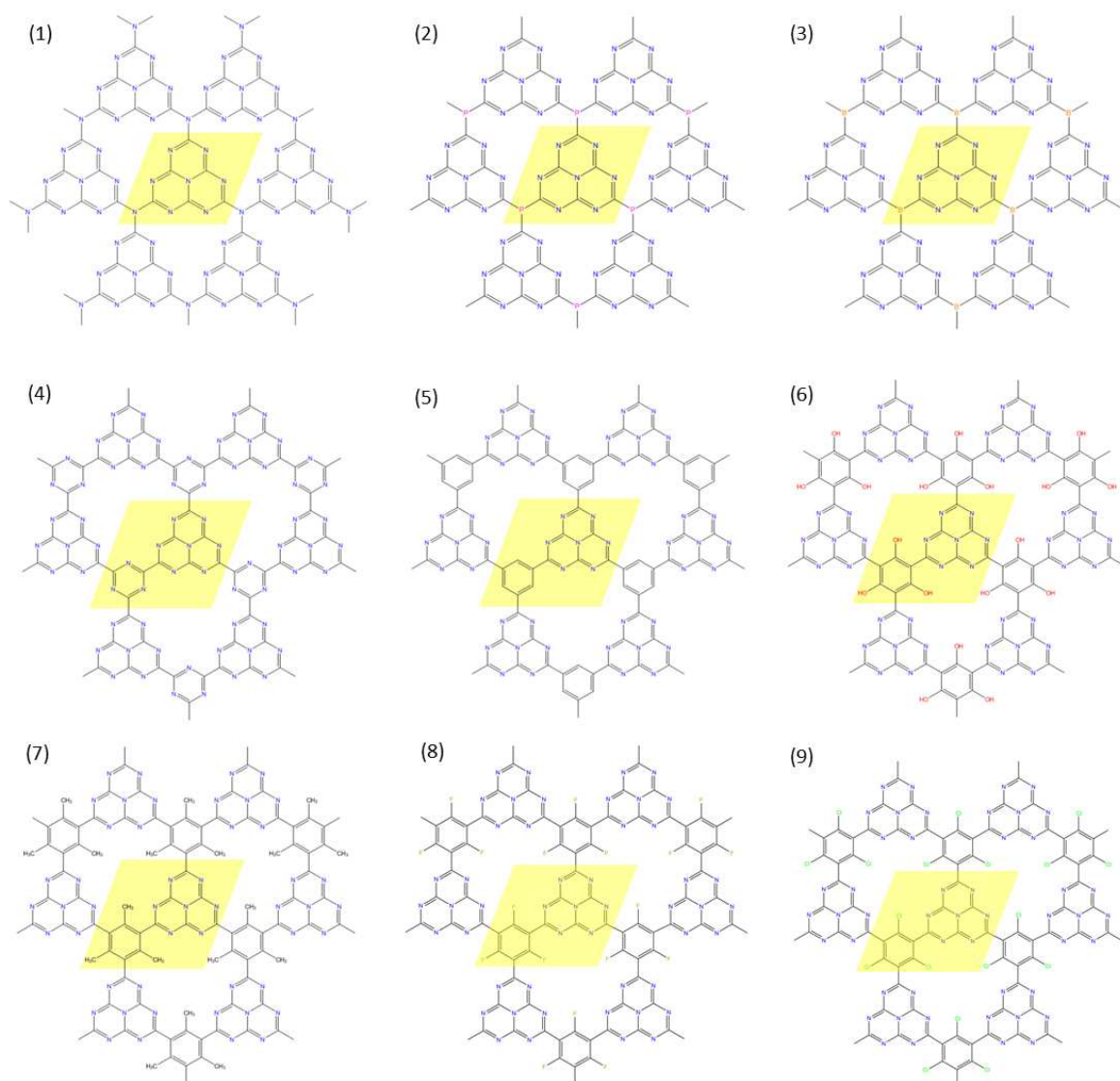
Figure 1 Graphitic carbon nitride-based structures with various linker units investigated in this work: (1) linker = nitrogen, (2) linker = phosphorus, (3) linker = boron, (4) linker = triazine, (5) linker = benzene, (6) linker = 1,3,5-trihydroxybenzene, (7) linker = 1,3,5-trimethylbenzene, (8) linker = 1,3,5-trifluorobenzene, (9) linker = 1,3,5-trichlorobenzene. Unit cells, consisting of a heptazine unit and a linker, are highlighted in yellow.

2. Computational details

2.1. Computational methods

The optimised geometries, wavefunctions and energies of all structures were obtained using density functional theory (DFT) calculations performed with the B3LYP hybrid functional[38] using the CRYSTAL09 package.[39] Carbon, nitrogen and oxygen atoms were described with 6-31G(d) basis sets, hydrogen atoms with 31G(p), phosphorus atoms with 8-5-21G(d) and boron atoms with 6-21G(d) basis sets. The basis sets were obtained from the CRYSTAL online database.[40] Grimme's D2 dispersion correction was applied.[41] Anderson mixing with the

mixing parameter of 0.95 was used; in cases of poor convergence the mixing parameter was increased up to 0.99. Two-dimensional (2D) and three-dimensional (3D) structures were modelled using periodic boundary conditions. 2x2x1 and 2x2x2 k-point grids were used during optimisation of 2D and 3D structures, respectively; while 12x12x1 and 12x12x12 grids were used in subsequent calculations of the densities of states. All structures were fully optimised. No symmetry constraints were applied, to avoid enforcing particular types of symmetry, e.g. planarity. Lattice parameters were optimised for each 2D structure by doing a series of calculations with systematic variation of the in-plane lattice parameter a (first on a 0.1 Å grid, then on a 0.01 Å grid) to identify the energy minimum; the angle was kept at 60° to maintain the hexagonal lattice. The lattice parameter c (separation between layers) for 3D structures was optimised in a similar way, using first a 0.1 Å grid and then a 0.01 Å grid of values of c.

Densities of states (DOS) and band structures were plotted with CRYSTAL's post-processing tools, using optimised wavefunctions. Absolute orbital energies of 2D structures are reported relative to the vacuum level (the energy of electron in vacuum). For accurate determination of absolute orbital energies, electrostatic potential in vacuum above and below the 2D sheets was calculated; the magnitude of the electrostatic potential was always very small, below 0.01 V (except structures 2 and 7, where the potentials were ±0.11 V and ±0.05 V, respectively, i.e. still very small). Therefore orbital energies and densities of states of the 2D structures are reported without further corrections. To obtain the values of orbital energies of 3D structures relative to the vacuum level, N 1s core levels of the 3D structures were aligned with the corresponding core levels of the corresponding 2D structures, on assumption that core levels are only weakly affected by weak interlayer interactions.

2.2. Construction of 3D structures

To investigate the effect of stacking of 2D sheets on interlayer binding and electronic properties, two types of stacking were considered. First, AA stacking was considered, where each layer is directly above the previous layer (Figure 2(a,c)). Second, AB stacking (Figure 2(b)), similar to in the AB stacking in graphite, was considered. Here, each next layer is shifted relative to the layer below it by the same amount, 1.41 Å (similar to the shift in the AB stacking in graphite and close to the average value between the length of the C=N bond, 1.33 Å, and the length of the C-N bond, 1.46 Å), so that some of the C and N atoms are above C or N atoms of the layer below, while other atoms are above hexagons of centres of pores (Figure 2(b,d)). However, unlike the AB stacking in graphite, the stacking considered here does not result in all odd-numbered layers and all even-numbered layers being equivalent to each other; instead, each subsequent layer is shifted by the same amount. ABAB stacking, more akin to graphite, where all odd-numbered layers are directly above each other and all even-numbered layers are similarly directly above each other, is also

a possibility, although a full exploration of all possible stacking combinations is beyond the scope of this work. Both AA, AB and ABAB stacking, as well as various intermediate stacking types (e.g. various combinations of AB and ABAB where subsequent layers may be shifted in different directions), are expected to co-exist in real materials, which are known to be disordered.[4]
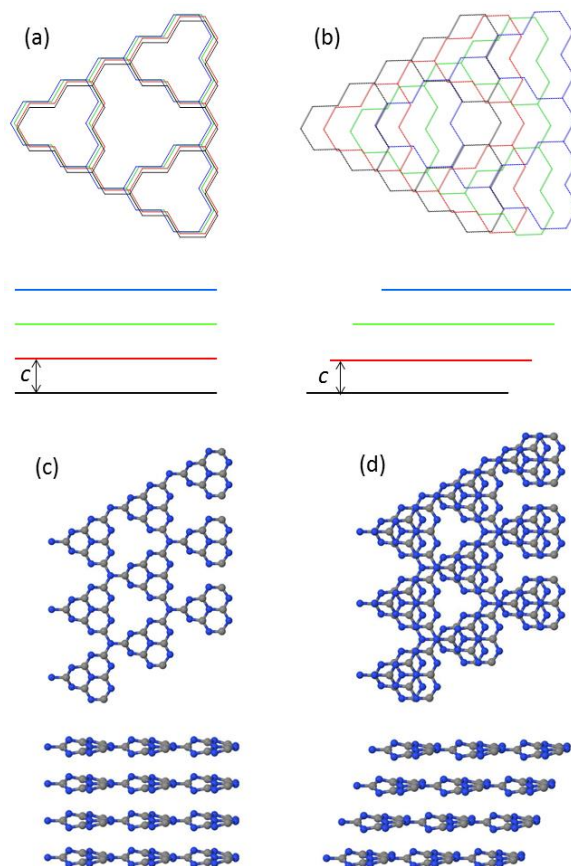
Figure 2 (a,b) Schematic images of (a) AA and (b) AB stacking in graphitic carbon nitride, showing four consecutive layers: layer 1 - in black, 2 - red, 3 - green, 4 - blue. In (a), each layer is directly above the previous layer. In (b), each layer is shifted by the same amount with respect to the previous layer. (c, d) Optimised structures of the N-linked carbon nitride: (c) AA stacking, (d) AB stacking (top and side views). The top view in (d) shows only two layers, for clarity.

3. Results and discussion

3.1. Structures and interaction energies

The optimised structures and their 3D stacking are shown in Figures 3 and 4. Table 1 shows the optimised lattice parameters and interlayer binding energies. The in-plane lattice parameter a for the N-linked g-C_3N_4 structure (Figure 1(a) and Figure 2(c)), 6.94 Å, is consistent with the previously reported experimental values (6.81 Å)[8] and calculated values (7.06-7.16 Å).[42-44] The lattice parameters for the P- and B-linked structures are slightly larger, consistent with the longer

ARTICLE

C-P and C-B bonds (1.83 and 1,61 Å, respectively, cf. 1.46 Å for the C-N bond). The lattice parameters *a* for the benzene- and triazine-linked structures, between 9.4-9.7 Å, are larger because of the larger size of these linker groups compared to single atoms.

Table 1 Lattice parameters and interlayer interaction energies for structures 1-9. (No planar AB-stacked structures were obtained for 2b and 3b.)

Structure	Linker	Planarity	*a*, Å	*c*, Å		Eint, meV/atom	
				AA	AB	AA	AB
1	N	non-planar	6.94	3.58	3.37	-46	-68
2a	P	non-planar	7.56	3.71	3.51	-50	-54
2b	P	planar	7.65	3.96	-	-17	-
3a	B	non-planar	7.29	3.44	3.69	-47	-57
3b	B	planar	7.42	3.40	-	-24	-
4	triazine	planar	9.41	3.85	3.26	-13	-44
5	benzene	planar	9.56	3.77	3.13	-24	-59
6	1,3,5-trihydroxy-benzene	planar	9.67	3.65	3.08	-29	-61
7	1,3,5-trimethyl-benzene	non-planar	9.43	3.60	3.85	-59	-46
8	1,3,5-trifluoro-benzene	non-planar	9.55	3.60	3.40	-33	-47
9	1,3,5-trichloro-benzene	non-planar	9.45	3.86	3.90	-47	-39

Notably, some of the structures are planar while others are non-planar. The g-C_3N_4 structure (Figure 1(a)) is buckled, in agreement with previous computational studies.[42, 44] This is attributed to the sp^3 hybridisation of the linker nitrogen atoms. Structures containing triazine, benzene and trihydroxybenzene linkers are planar (Figure 4). In contrast, structures containing methyl- and halogen-substituted benzene linkers are non-planar, even though their starting geometries before optimisation were planar. This non-planarity is attributed to steric effects (for the trimethylbenzene-linked structure) and electronic repulsion between electronegative halogen and nitrogen atoms (halogen-substituted structures). In the hydroxyl-substituted structure, hydrogen bonding between heptazine nitrogens and hydroxyl hydrogens favours planarity of the structure. For the phosphorus and boron-substituted structures, both planar and nonplanar geometries were obtained (Figure 3). However, the planar geometries were always less stable and were isolated only for 2D and AA-stacked 3D systems, while the corresponding AB-stacked systems spontaneously became non-planar, similar to the g-C_3N_4 structure.

The interlayer spacing for N-linked g-C_3N_4 was calculated as *c* = 3.37 Å for the AB-stacked system, in good agreement with the experimental value of 3.26 Å.[8] The AA-stacked g-C_3N_4 system has a larger lattice interlayer spacing of 3.58 Å. A similar pattern is observed across all structures: interlayer spacings are typically larger for AA-stacked systems than for AB-stacked systems. The spacings are the lowest for planar AB-stacked structures (triazine, benzene and trihydroxybenzene-linked): *c* = 3.08-3.26 Å, lower than in g-C_3N_4 and lower than the graphite interlayer spacing of 3.35 Å.[45] Non-planar structures generally have smaller differences in interlayer spacings between different stacking types.

These interlayer distances can be correlated to the calculated interlayer interaction energies (Table 1). The interaction energies are all negative, indicating favourable interaction between layers, and range between -13 – -68 meV/atom (not including H atoms). This energy range is similar to graphite interlayer interaction energies of -35 – -51 meV/atom,[46-48] suggesting that the nature of the interaction is similar to that in graphite. AB-stacked systems are typically more strongly bound than AA-stacked ones, consistent with the smaller interlayer spacings for the AB-stacked systems. This is particularly clear for the planar organic-linked structures 4, 5, 6: AB-stacked systems are more stable than AA by 31-36 meV/atom, similar to the behaviour of graphite and benzene dimer,[47-49] where the AA stacking causes repulsive interaction between the π-orbitals, while AB stacking (or shifted benzene dimer) insures favourable overlap of the π-orbitals. The situation is similar for N-, B- and P-linked systems, where AB-stacked structures are more stable by 5-22 meV/atom (larger energy difference for the small N linker, smaller difference for the large P linker). Non-planar organic-linked structures have a less clear pattern of interaction energies; in particular, bulky

substituents (Cl and methyl) make the AA-stacked systems more favourable. This is because in these systems, repulsion between bulky groups becomes significant, and the AA stacking where such groups can avoid each other outweighs favourable electronic interaction between π-orbitals provided by the AB stacking. Because of the similarities of the interaction energies for the two stacking types in non-planar organic-linked structures 7-9, a variety of stacking types are expected to co-exist (both AA, AB and possibly some other less regular stacking types, with amounts of shift intermediate between AA and AB). Similarly, for P- and B-linked structures 2 and 3, a variety of stacking types of non-planar structures are expected to co-exist, while the planar structures are metastable and are expected to become non-planar. For the planar organic-linked structures 4-6 and for the N-linked g-C_3N_4, there is a clear energetic preference for the AB-stacked structures to form.
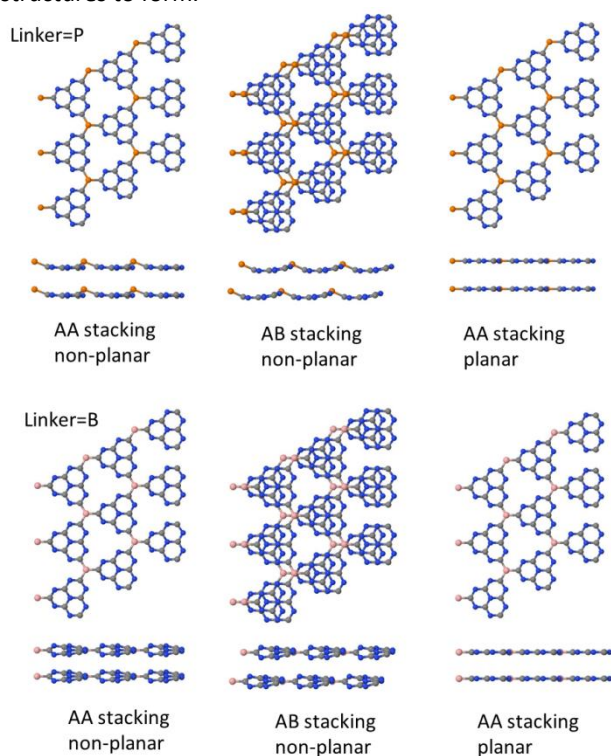

Figure 3 Optimised structures of P-linked (top row) and B-linked (bottom row) graphitic carbon nitride. Two layers of the 3D structures are shown. In AA stacking, each layer is directly above the previous layer, therefore only the top layer is visible in the top view.
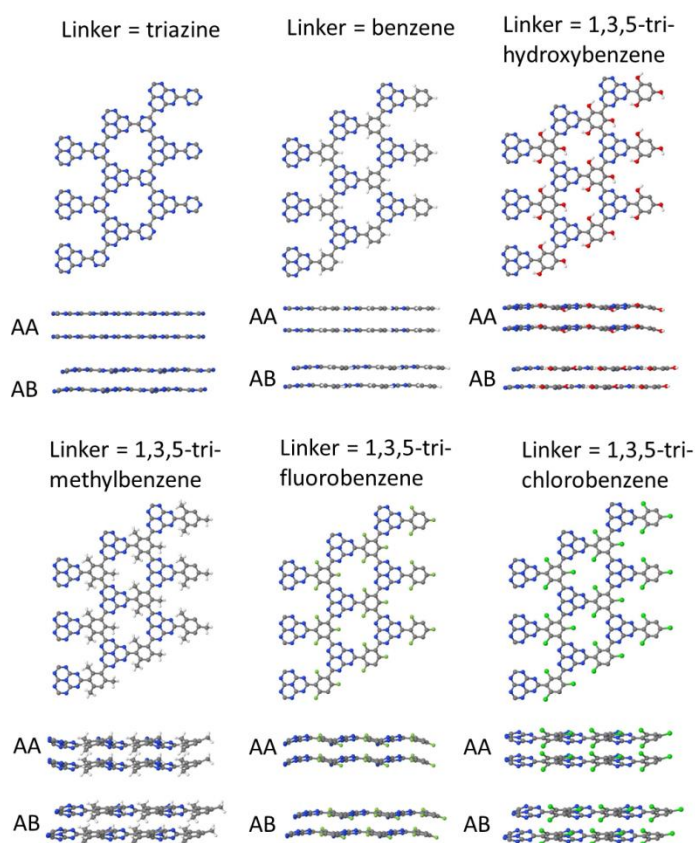

Figure 4 Optimised structures of triazine-, benzene- and substituted benzene-linked graphitic carbon nitride. The top views show only a single layer, for clarity. The side views show two layers of the 3D AA- and AB-stacked structures.

3.2. Electronic structure

3.2.1. Band gaps. The energies of valence band maxima (VBM) and conduction band minima (CBM) and the band gaps (calculated as the difference between CBM and VBM) of structures 1-9 are presented in Table 2, both for the 2D and 3D structures. Densities of states and band structures are presented in Figures S1-S4 in the Supplementary Information. The band gaps are typically indirect; in the few cases where the 2D structures have direct band gaps (structures 1, 2b, 3b), they become indirect in the corresponding 3D structures. As expected, the band gaps of the 3D systems are smaller than for 2D systems. For example, the 2D form of the nitrogen-linked structure has the calculated band gap of 3.31 eV, while the 3D AA- and AB-stacked systems have the band gaps of 3.05 and 2.94 eV, respectively. The 2.94 eV band gap value for the more stable AB stacking is close to to the experimentally measured band gap of g-C_3N_4, 2.7 eV.[8] The 0.3-0.4 eV increase in the band gap of the 2D structure compared to the 3D ones is comparable to the 0.2 eV increase reported experimentally for g-C_3N_4 nanosheets compared to the bulk material[26, 28-29] (however, multilayers containing ca. 7 layers rather than single layers were obtained in those works, possibly explaining the smaller increase in the band gap). The 0.24 eV difference between the experimental and calculated band gaps of the

bulk structure can be attributed to a combination of factors: (i) the fact that the band gap calculated as a difference of Kohn-Sham orbitals is only an approximation to the optical gap and does not involve exciton binding, (ii) the known tendency of hybrid DFT functionals, such as B3LYP, to overestimate band gaps,[50] and (iii) the fact that the true g-C_3N_4 structure is likely to contain chains of linked heptazines assembled into 2D sheets,[3, 19] rather than the fully condensed 2D sheets of heptazines considered here. The first two factors are expected to artificially increase the calculated band gap, while the use of the fully condensed g-C_3N_4 is expected to decrease the calculated gap; thus the 0.24 eV difference between the calculated and experimental band gap reflects the balance of these factors. This serves as an approximate measure of accuracy of our calculated band gap: we expect that the band gaps of the new structures predicted in this work may be ≈0.2 eV overestimated.

Table 2 Electronic properties of the carbon nitride-based 2D and 3D structures: band gap energies, direct (d) or indirect (i) nature of the gap, and positions of the VBM and CBM on the absolute scale (relative to the energy of electron in vacuum) and on the electrochemical scale (relative to the normal hydrogen electrode).

Structure	Linker	Stacking	Eg, eV	Direct or indirect gap	Band energies vs vacuum, eV		Band energies vs NHE, eV	
					VBM	CBM	VBM	CBM
1	N	2D	3.31	d	-6.41	-3.10	1.97	-1.34
		AA	3.05	d	-6.32	-3.28	1.88	-1.16
		AB	2.94	i	-6.19	-3.25	1.75	-1.19
2a	P (nonplanar)	2D	3.32	i	-6.57	-3.25	2.13	-1.19
		AA	2.63	i	-6.26	-3.63	1.82	-0.81
		AB	2.86	i	-6.39	-3.53	1.95	-0.91
2b	P (planar)	2D	3.14	d	-6.43	-3.29	1.99	-1.15
		AA	2.27	i	-5.80	-3.53	1.36	-0.91
		AB	--	--	--	--	--	--
3a	B (nonplanar)	2D	1.74	i	-6.35	-4.61	1.91	0.17
		AA	0.96	i	-6.35	-5.39	1.91	0.95
		AB	1.59	i	-6.20	-4.61	1.76	0.17
3b	B (planar)	2D	1.47	d	-6.05	-4.58	1.61	0.14
		AA	0.06	i	-5.67	-5.61	1.23	1.17
		AB	--	--	--	--	--	--
4	triazine	2D	2.99	i	-6.89	-3.91	2.45	-0.53
		AA	2.45	i	-6.69	-4.24	2.25	-0.20
		AB	2.74	i	-6.81	-4.07	2.37	-0.37
5	benzene	2D	3.52	i	-6.68	-3.16	2.24	-1.28
		AA	2.88	i	-6.45	-3.57	2.01	-0.87
		AB	2.98	i	-6.44	-3.46	2.00	-0.98
6	1,3,5-trihydroxybenzene	2D	3.24	i	-6.30	-3.06	1.86	-1.38
		AA	2.45	i	-5.88	-3.43	1.44	-1.01
		AB	2.70	i	-5.86	-3.16	1.42	-1.28
7	1,3,5-trimethylbenzene	2D	3.42	i	-6.41	-2.99	1.97	-1.45
		AA	3.17	i	-6.15	-2.98	1.71	-1.46
		AB	3.21	i	-6.18	-2.97	1.74	-1.47
8	1,3,5-trifluorobenzene	2D	3.38	d	-6.83	-3.45	2.39	-0.99
		AA	3.23	i	-6.78	-3.56	2.34	-0.88
		AB	3.08	i	-6.70	-3.62	2.26	-0.82
9	1,3,5-trichlorobenzene	2D	3.14	i	-6.73	-3.59	2.29	-0.85
		AA	3.03	i	-6.60	-3.57	2.16	-0.87
		AB	2.83	i	-6.46	-3.62	2.02	-0.82

Our results also enable us to make qualitative comparisons of the effects of various linker groups on the band gaps. For example, phosphorus doping slightly reduces the band gap compared to g-C_3N_4, in particular in 3D systems (by 0.1-0.4 eV), because of a downward shift of the CB, which is possibly caused by the P atom contributing both to the VBM and the CBM (Figure S1). Thus, phosphorus-linked structures are expected to absorb light in the visible range and have better light-harvesting ability than g-C_3N_4.

Boron doping dramatically reduces the band gap to 1.74 eV (the nonplanar 2D structure) and 1.59 eV (the most stable AB-stacked 3D structure), corresponding to absorption of red light; the calculated band gaps of the less stable AA-stacked B-linked structures are even lower, 0.96 and 0.06 eV for the non-planar and planar structures, respectively. This reduction in

the band gap is caused by the presence of the lowest unoccupied band localised on boron (Figure S1; the high dispersion of this band is seen in the band structure plots in Figure S3). Since this CB is predominantly formed by boron orbitals, while the VBM is formed predominantly by the heptazine nitrogens, the VB to CB optical excitation is expected to be very weak; however, the boron-based CB is expected to be a trap state to trap photoexcited electrons decaying from higher bands and thus to reduce electron-hole recombination. Thus, boron-linked carbon nitride structures are expected both to be able to absorb visible light and to have favourable electron-hole separation compared to g-C$_3$N$_4$.

All planar 3D organic-linked structures (with triazine, benzene and hydroxyl-substituted benzene linkers) have the band gaps lower than those of the N-linked g-C$_3$N$_4$, up to 2.45 eV (green light) for the triazine-linked and trihydroxybenzene-linked AA-stacked structures. This is attributed to better electronic conjugation between the heptazines and linker groups. Notably, all organic-linked structures have significant contributions of the linker groups in their VBM and, in some cases, CBM (Figure S2), which is likely responsible for the lower-lying CBM (triazine- and benzene-linked structures) and higher-lying VBM (trihydroxybenzene-linked structure). Thus these organic-linked structures are expected to have better light-harvesting abilities than g-C$_3$N$_4$; this also suggests more generally that planar organic covalent heptazine-based structures, similar to covalent triazine frameworks,[22-23] should have favourable light-harvesting abilities.

In contrast, non-planar organic-linked structures (containing fluoro-, chloro- and methyl-substituted benzene linkers) have the band gaps similar and even slightly larger (by up to 0.3 eV) than the N-linked structures. Therefore the presence of an organic linker group is not a sufficient requirement for achieving a small band gap; the structure should be planar to achieve favourable interaction of the π-electron systems of the 2D layers. Notably, the non-planar organic-linked 3D structures had only a small reduction of the band gap compared to their 2D forms (by 0.1-0.3 eV); this suggests weak electronic interaction of the π-conjugated groups forming the CBM and VBM and is consistent with their large interlayer spacing (Table 1). By comparison, the planar organic-linked 3D structures showed large reduction in the band gaps of their 3D forms compared to the 2D forms (by 0.25-0.8 eV) this, together with these structures' small interlayer spacings, indicates strong electronic interaction between layers.

3.2.1. Band energies and implication for photocatalytic properties. For application in photocatalysis, a narrow band gap suitable for efficient harvesting of visible light is not sufficient; the photocatalyst material's CB and VB should also be suitably positioned to provide electrons and holes for photo-reduction and photo-oxidation processes, respectively. The conduction band minimum should be sufficiently high, or, in other words, it should correspond to a more negative potential than the redox potential of the desired reduction process. Similarly, the VBM should be low and correspond to a

more positive potential than the redox potential of the desired oxidation process. The potential on the absolute scale where zero is the energy of electron in vacuum (E_{vac}) is related to the electrochemical scale, relative to the normal hydrogen electrode (NHE) (E_{NHE}), as: $E_{NHE} = - E_{vac}$ - 4.44 V. E_{vac} and E_{NHE} are shown as the two vertical axes in Figure 5.

For application in photocatalytic water splitting, the photocatalysts's CBM should be more electronegative (more negative in potential, or higher in absolute energy) than the H$^+$/H$_2$ reduction potential (0 V with respect to the NHE), while the VBM should be more electropositive (more positive in potential, or lower in absolute energy) than the OH$^-$/O$_2$ oxidation potential (1.23 V wrt. NHE). Moreover, redox processes typically involve overpotentials, i.e. require potentials larger than the ideal values, therefore in practice the CBM should be more electronegative, and the VBM should be more electropositive than the respective ideal thermodynamic values of 0 V and 1.23 V.[4]

Table 2 and Figure 5 show the band energies of the studied materials both on the absolute scale, and on the electrochemical scale (relative to NHE), and compare them to the experimental values (where available) and to the ideal values of the water oxidation and reduction potentials. The calculated band edge positions of the N-linked material (VBM at -6.19 eV wrt. the vacuum level, or 1.75 V wrt. NHE, and CBM at -3.25 eV wrt. the vacuum level, -1.19 V wrt. NHE) can be compared to the experimentally measured values for bulk g-C$_3$N$_4$: VBM at 1.83 V and CBM at -0.83 V wrt. NHE.[25] The VBM energy is accurately predicted by our calculations, while the CBM position is slightly overestimated (by 0.36 eV), consistent with the slightly overestimated calculated band gap. For g-C$_3$N$_4$ nanosheets, experiments report VBM to be the same as for bulk g-C$_3$N$_4$, and CBM to be 0.09-0.17 eV higher than for the bulk material;[28-29] our calculations are in reasonable agreement with these results, showing a slight downshift of the VBM (0.22 eV) and a slight upshift of the CBM (0.15 eV) relative to the calculated bulk values. Thus, the calculated values of VBM and CBM can be considered reliable, within the computational uncertainty of up to 0.4 eV. Both the calculated and the available experimental values[25] agree that this material's CBM is suitably positioned to reduce hydrogen to H$_2$, and the VBM is suitably positioned to oxidise water to O$_2$: the CBM and VBM straddle the water reduction and oxidation potential and additionally provide sufficient overpotential for water splitting (i.e. both the water oxidation and reduction reactions) to take place.

As seen in Figure 5, the band positions are similar for most of the other materials studied in this work: the P-linked structure and all organic-linked structures have sufficiently energetic VB and CB to photocatalyse both water oxidation and reduction, and they provide sufficient overpotential for both the oxidation and reduction processes. Band positions of the P-linked structure are also in good agreement with available experimental data:[34] with there being only a small downshift of the VBM (-0.18 eV calculation, -0.09 eV experiment) and a slightly larger upshift of the CBM (0.28

eV calculation, 0.14 eV experiment) of the 2D structure compared to the bulk material. Notably, several of these materials have highly positive VB potentials favourable for water oxidation (triazine-, benzene-, chloro- and fluorobenzene-linked materials); this is particularly important since water oxidation has been much more challenging to achieve than hydrogen reduction.[17-18]

Slight outliers among these systems are the triazine-linked material and the trihydroxybenzene-linked material. The triazine-linked material has the VBM that is sufficiently energetic for water oxidation, but its CBM is only 0.2-0.5 eV above the water reduction potential. Considering the need for overpotential and the possible overestimation of the CBM in our calculations, it is possible that the CBM or the triazine-linked material is not sufficiently energetic to catalyse water reduction. The trihydroxybenzene-linked material, on the contrary, has a suitable CBM for hydrogen reduction, but its VBM may be unable to provide sufficient overpotential for water oxidation.

The B-linked structure is a more unusual case: its VBM is low enough to oxidise water (1.23-1.91 V wrt. NHE), but its CBM is below the water reduction potential. Thus, this material is not expected to reduce water to hydrogen, and therefore is unable to photocatalyse the complete water splitting process. However, this material can still be used in a photocatalytic Z-scheme, i.e. a combination of two photocatalysts such that one is responsible for the oxidation process and the other is responsible for the reduction process.[51-52] Keeping in mind the small band gap of this material and the possibility for absorbing light in the whole visible range up to red, this materials seems a promising photocatalyst for water oxidation.
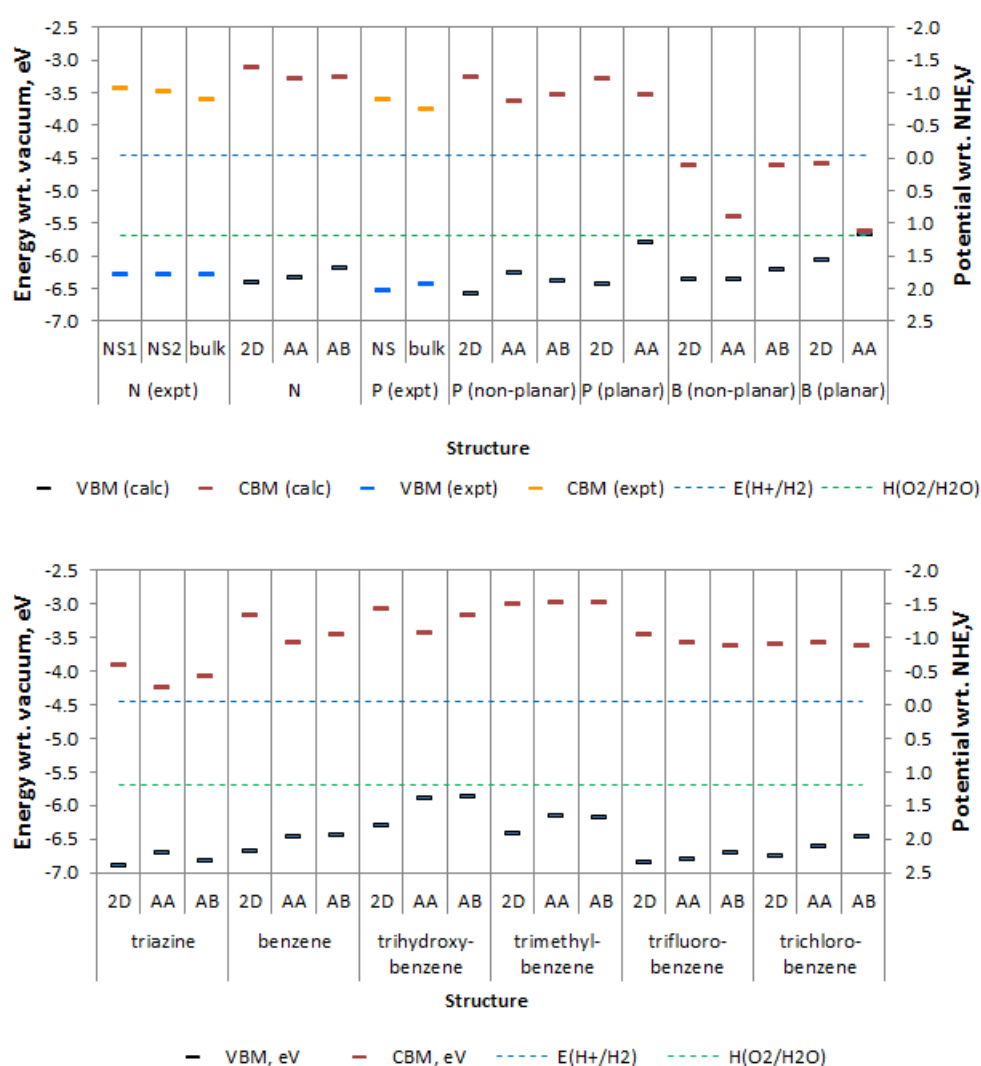

Figure 5 Positions of valence band maxima and conduction band minima of structures 1-3 (top) and 4-9 (bottom) on the absolute scale (relative to the energy of the electron in vacuum) and on the electrochemical scale (relative to the energy of the normal hydrogen electrode). The redox potential for the water reduction (H^+/H_2) and oxidation (O_2/H_2O) processes, relative to the NHE at pH 0, are shown for comparison. Experimental data from the literature for bulk g-C_3N_4[25] and g-C_3N_4 nanosheets (NS1[28] & NS2[29]) and for phosphorous-doped bulk material and phosphorus-doped nanosheets (NS)[34] are included. No experimental band positions data were found for the other doped or modified structures.

ARTICLE

4. Conclusions

A range of modifications to the standard g-C$_3$N$_4$ structure were considered in this work, using density-functional theory calculations. The nitrogen linker was systematically replaced with other trivalent atoms (phosphorus, boron) and three-coordinated organic fragments (triazine, benzene and substituted benzenes). The effect of different stacking of the 2D sheets of these materials on their geometries, interaction energies and electronic properties was considered. Our calculations show that the chemical nature of the materials has a significant effect on their geometry (planarity, interlayer spacing). In particular, planar structures (triazine-, benzene- and trihydroxybenzene-linked carbon nitrides) and the N-linked g-C$_3$N$_4$ show strong energetic preference for the AB stacking, while the non-planar structures have no strong preference towards a particular stacking and are expected to adopt a variety of stacking types (AA, AB and intermediate types).

The chemical nature and the 2D or 3D arrangements of the studied materials have a significant effect on their electronic properties. Thus, the 3D structures always have lower band gaps than their 2D counterparts, which is expected to result in improved light harvesting. Chemical modifications of the N-linked g-C$_3$N$_4$ by replacing the nitrogen linker atom typically lead to a reduction in the band gap, in particular for the phosphorus-linked and the planar triazine-, benzene- and trihydroxybenzene-linked materials. The band gap narrowing is particularly pronounced in the boron-linked material: this structure is expected to be able to absorb light in the whole of the visible range. This impact on the electronic properties has significant implications for photocatalytic abilities of these materials. The lower band gaps are expected to result in improved light harvesting properties of the new materials compared to the standard g-C$_3$N$_4$. All the materials considered here (with the exception of the B-linked material) have the valence and conduction bands suitably positioned to photocatalyse both the water oxidation and reduction processes, i.e. in principle all these materials should be able to drive direct water splitting. The exception is the B-linked material, which is expected to be active only for water oxidation. Thus, our computational study shows that chemical modification of g-C$_3$N$_4$ is a powerful method to tune this material's electronic properties and improve its photocatalytic activity. The most promising materials, in terms of their potential light absorption and water oxidation and reduction abilities, are the P- and B-doped and the organic triazine-, benzene- and trihydroxybenzene-linked materials. We suggest that these structures warrant further experimental investigation.

Conflicts of interest

There are no conflicts to declare.

Acknowledgements

References

1. Liebig, J., Uber einige Stickstoff - Verbindungen. *Annalen der Pharmacie* **1834,** *10* (1), 1-47.
2. Teter, D. M.; Hemley, R. J., Low-Compressibility Carbon Nitrides. *Science* **1996,** *271* (5245), 53.
3. Fina, F.; Callear, S. K.; Carins, G. M.; Irvine, J. T. S., Structural Investigation of Graphitic Carbon Nitride via XRD and Neutron Diffraction. *Chemistry of Materials* **2015,** *27* (7), 2612-2618.
4. Wang, X.; Blechert, S.; Antonietti, M., Polymeric Graphitic Carbon Nitride for Heterogeneous Photocatalysis. *ACS Catalysis* **2012,** *2* (8), 1596-1606.
5. Wang, Y.; Wang, X.; Antonietti, M., Polymeric Graphitic Carbon Nitride as a Heterogeneous Organocatalyst: From Photochemistry to Multipurpose Catalysis to Sustainable Chemistry. *Angewandte Chemie International Edition* **2012,** *51* (1), 68-89.
6. Zhao, Z.; Sun, Y.; Dong, F., Graphitic carbon nitride based nanocomposites: a review. *Nanoscale* **2015,** *7* (1), 15-37.
7. Mishra, A.; Mehta, A.; Basu, S.; Shetti, N. P.; Reddy, K. R.; Aminabhavi, T. M., Graphitic carbon nitride (g–C3N4)–based metal-free photocatalysts for water splitting: A review. *Carbon* **2019,** *149*, 693-721.
8. Wang, X.; Maeda, K.; Thomas, A.; Takanabe, K.; Xin, G.; Carlsson, J. M.; Domen, K.; Antonietti, M., A metal-free polymeric photocatalyst for hydrogen production from water under visible light. *Nature Materials* **2009,** *8* (1), 76-80.
9. Acar, C.; Dincer, I.; Naterer, G. F., Review of photocatalytic water-splitting methods for sustainable hydrogen production. *International Journal of Energy Research* **2016,** *40* (11), 1449-1473.
10. Ismail, A. A.; Bahnemann, D. W., Photochemical splitting of water for hydrogen production by photocatalysis: A review. *Solar Energy Materials and Solar Cells* **2014,** *128*, 85-101.
11. Corredor, J.; Rivero, M. J.; Rangel, C. M.; Gloaguen, F.; Ortiz, I., Comprehensive review and future perspectives on the photocatalytic hydrogen production. *Journal of Chemical Technology & Biotechnology* **2019,** *94* (10), 3049-3063.
12. Kudo, A.; Miseki, Y., Heterogeneous photocatalyst materials for water splitting. *Chemical Society Reviews* **2009,** *38* (1), 253-278.

13. Maeda, K.; Domen, K., Photocatalytic Water Splitting: Recent Progress and Future Challenges. *The Journal of Physical Chemistry Letters* **2010,** *1* (18), 2655-2661.

14. Schneider, J.; Bahnemann, D. W., Undesired Role of Sacrificial Reagents in Photocatalysis. *The Journal of Physical Chemistry Letters* **2013,** *4* (20), 3479-3483.

15. Etacheri, V.; Di Valentin, C.; Schneider, J.; Bahnemann, D.; Pillai, S. C., Visible-light activation of TiO2 photocatalysts: Advances in theory and experiments. *Journal of Photochemistry and Photobiology C: Photochemistry Reviews* **2015,** *25*, 1-29.

16. Willkomm, J.; Orchard, K. L.; Reynal, A.; Pastor, E.; Durrant, J. R.; Reisner, E., Dye-sensitised semiconductors modified with molecular catalysts for light-driven H2 production. *Chemical Society Reviews* **2016,** *45* (1), 9-23.

17. Zhang, G.; Lan, Z.-A.; Lin, L.; Lin, S.; Wang, X., Overall water splitting by Pt/g-C3N4 photocatalysts without using sacrificial agents. *Chemical Science* **2016,** *7* (5), 3062-3066.

18. Liu, J.; Liu, Y.; Liu, N.; Han, Y.; Zhang, X.; Huang, H.; Lifshitz, Y.; Lee, S.-T.; Zhong, J.; Kang, Z., Metal-free efficient photocatalyst for stable visible water splitting via a two-electron pathway. *Science* **2015,** *347* (6225), 970.

19. Lotsch, B. V.; Döblinger, M.; Sehnert, J.; Seyfarth, L.; Senker, J.; Oeckler, O.; Schnick, W., Unmasking Melon by a Complementary Approach Employing Electron Diffraction, Solid-State NMR Spectroscopy, and Theoretical Calculations—Structural Characterization of a Carbon Nitride Polymer. *Chemistry – A European Journal* **2007,** *13* (17), 4969-4980.

20. Kroke, E.; Schwarz, M.; Horath-Bordon, E.; Kroll, P.; Noll, B.; Norman, A. D., Tri-s-triazine derivatives. Part I. From trichloro-tri-s-triazine to graphitic C3N4 structures. *New Journal of Chemistry* **2002,** *26* (5), 508-512.

21. Algara-Siller, G.; Severin, N.; Chong, S. Y.; Björkman, T.; Palgrave, R. G.; Laybourn, A.; Antonietti, M.; Khimyak, Y. Z.; Krasheninnikov, A. V.; Rabe, J. P.; Kaiser, U.; Cooper, A. I.; Thomas, A.; Bojdys, M. J., Triazine-Based Graphitic Carbon Nitride: a Two-Dimensional Semiconductor. *Angewandte Chemie International Edition* **2014,** *53* (29), 7450-7455.

22. Jiang, X.; Wang, P.; Zhao, J., 2D covalent triazine framework: a new class of organic photocatalyst for water splitting. *Journal of Materials Chemistry A* **2015,** *3* (15), 7750-7758.

23. Sakaushi, K.; Antonietti, M., Carbon- and Nitrogen-Based Organic Frameworks. *Accounts of Chemical Research* **2015,** *48* (6), 1591-1600.

24. Vinu, A.; Ariga, K.; Mori, T.; Nakanishi, T.; Hishita, S.; Golberg, D.; Bando, Y., Preparation and Characterization of Well-Ordered Hexagonal Mesoporous Carbon Nitride. *Advanced Materials* **2005,** *17* (13), 1648-1652.

25. Zhang, Y.; Antonietti, M., Photocurrent Generation by Polymeric Carbon Nitride Solids: An Initial Step towards a Novel Photovoltaic System. *Chemistry – An Asian Journal* **2010,** *5* (6), 1307-1311.

26. Niu, P.; Zhang, L.; Liu, G.; Cheng, H.-M., Graphene-Like Carbon Nitride Nanosheets for Improved Photocatalytic Activities. *Advanced Functional Materials* **2012,** *22* (22), 4763-4770.

27. Zhang, X.; Xie, X.; Wang, H.; Zhang, J.; Pan, B.; Xie, Y., Enhanced Photoresponsive Ultrathin Graphitic-Phase C3N4 Nanosheets for Bioimaging. *Journal of the American Chemical Society* **2013,** *135* (1), 18-21.

28. Li, X.; Hartley, G.; Ward, A. J.; Young, P. A.; Masters, A. F.; Maschmeyer, T., Hydrogenated Defects in Graphitic Carbon Nitride Nanosheets for Improved Photocatalytic Hydrogen Evolution. *The Journal of Physical Chemistry C* **2015,** *119* (27), 14938-14946.

29. Lin, Q.; Li, L.; Liang, S.; Liu, M.; Bi, J.; Wu, L., Efficient synthesis of monolayer carbon nitride 2D nanosheet with tunable concentration and enhanced visible-light photocatalytic activities. *Applied Catalysis B: Environmental* **2015,** *163*, 135-142.

30. Yan, S. C.; Li, Z. S.; Zou, Z. G., Photodegradation of Rhodamine B and Methyl Orange over Boron-Doped g-C3N4 under Visible Light Irradiation. *Langmuir* **2010,** *26* (6), 3894-3901.

31. Da Silva, E. S.; Moura, N. M. M.; Coutinho, A.; Dražić, G.; Teixeira, B. M. S.; Sobolev, N. A.; Silva, C. G.; Neves, M. G. P. M. S.; Prieto, M.; Faria, J. L., β-Cyclodextrin as a Precursor to Holey C-Doped g-C3N4 Nanosheets for Photocatalytic Hydrogen Generation. *ChemSusChem* **2018,** *11* (16), 2681-2694.

32. Wang, Y.; Bayazit, M. K.; Moniz, S. J. A.; Ruan, Q.; Lau, C. C.; Martsinovich, N.; Tang, J., Linker-controlled polymeric photocatalyst for highly efficient hydrogen evolution from water. *Energy & Environmental Science* **2017,** *10* (7), 1643-1651.

33. Wang, Y.; Di, Y.; Antonietti, M.; Li, H.; Chen, X.; Wang, X., Excellent Visible-Light Photocatalysis of Fluorinated Polymeric Carbon Nitride Solids. *Chemistry of Materials* **2010,** *22* (18), 5119-5121.

34. Ran, J.; Ma, T. Y.; Gao, G.; Du, X.-W.; Qiao, S. Z., Porous P-doped graphitic carbon nitride nanosheets for synergistically enhanced visible-light photocatalytic H2 production. *Energy & Environmental Science* **2015,** *8* (12), 3708-3717.

35. Hong, J.; Xia, X.; Wang, Y.; Xu, R., Mesoporous carbon nitride with in situ sulfur doping for enhanced photocatalytic hydrogen evolution from water under visible light. *Journal of Materials Chemistry* **2012,** *22* (30), 15006-15012.

36. Liu, C.; Zhang, Y.; Dong, F.; Reshak, A. H.; Ye, L.; Pinna, N.; Zeng, C.; Zhang, T.; Huang, H., Chlorine intercalation in graphitic carbon nitride for efficient photocatalysis. *Applied Catalysis B: Environmental* **2017,** *203*, 465-474.

37. Zhang, J.; Chen , X.; Takanabe, K.; Maeda, K.; Domen, K.; Epping, J. D.; Fu, X.; Antonietti, M.; Wang , X., Synthesis of a Carbon Nitride Structure for Visible-Light Catalysis by Copolymerization. *Angewandte Chemie International Edition* **2010,** *49* (2), 441-444.

38. Becke, A. D., Density-functional thermochemistry. III. The role of exact exchange. *The Journal of Chemical Physics* **1993,** *98* (7), 5648-5652.

39. Dovesi, R.; Orlando, R.; Civalleri, B.; Roetti, C.; Saunders Victor, R.; Zicovich-Wilson Claudio, M., CRYSTAL: a computational tool for the ab initio study of the electronic properties of crystals. In *Zeitschrift für Kristallographie - Crystalline Materials*, 2005; Vol. 220, p 571.

40. CRYSTAL - Basis Sets Library. http://www.crystal.unito.it/basis-sets.php (accessed 23/12/2019).

41. Grimme, S., Semiempirical GGA-type density functional constructed with a long-range dispersion correction. *Journal of Computational Chemistry* **2006,** *27* (15), 1787-1799.

42. Deifallah, M.; McMillan, P. F.; Corà, F., Electronic and Structural Properties of Two-Dimensional Carbon Nitride Graphenes. *The Journal of Physical Chemistry C* **2008,** *112* (14), 5447-5453.

43. Du, A.; Sanvito, S.; Li, Z.; Wang, D.; Jiao, Y.; Liao, T.; Sun, Q.; Ng, Y. H.; Zhu, Z.; Amal, R.; Smith, S. C., Hybrid Graphene and Graphitic Carbon Nitride Nanocomposite: Gap Opening, Electron–Hole Puddle, Interfacial Charge Transfer, and Enhanced Visible Light Response. *Journal of the American Chemical Society* **2012,** *134* (9), 4393-4397.

44. Ma, X.; Lv, Y.; Xu, J.; Liu, Y.; Zhang, R.; Zhu, Y., A Strategy of Enhancing the Photoactivity of g-C3N4 via Doping of Nonmetal Elements: A First-Principles Study. *The Journal of Physical Chemistry C* **2012,** *116* (44), 23485-23493.

45. Bernal, J. D.; Bragg, W. L., The structure of graphite. *Proceedings of the Royal Society of London. Series A, Containing Papers of a Mathematical and Physical Character* **1924,** *106* (740), 749-773.

46. Benedict, L. X.; Chopra, N. G.; Cohen, M. L.; Zettl, A.; Louie, S. G.; Crespi, V. H., Microscopic determination of the interlayer binding energy in graphite. *Chemical Physics Letters* **1998,** *286* (5), 490-496.

47. Lebedeva, I. V.; Knizhnik, A. A.; Popov, A. M.; Lozovik, Y. E.; Potapkin, B. V., Interlayer interaction and relative vibrations of bilayer graphene. *Physical Chemistry Chemical Physics* **2011,** *13* (13), 5687-5695.

48. Ziambaras, E.; Kleis, J.; Schröder, E.; Hyldgaard, P., Potassium intercalation in graphite: A van der Waals density-functional study. *Physical Review B* **2007,** *76* (15), 155425.

49. Tsuzuki, S.; Honda, K.; Uchimaru, T.; Mikami, M.; Tanabe, K., Origin of Attraction and Directionality of the π/π Interaction: Model Chemistry Calculations of Benzene Dimer Interaction. *Journal of the American Chemical Society* **2002,** *124* (1), 104-112.

50. Garza, A. J.; Scuseria, G. E., Predicting Band Gaps with Hybrid Density Functionals. *The Journal of Physical Chemistry Letters* **2016,** *7* (20), 4165-4170.

51. Li, H.; Tu, W.; Zhou, Y.; Zou, Z., Z-Scheme Photocatalytic Systems for Promoting Photocatalytic Performance: Recent Progress and Future Challenges. *Advanced Science* **2016,** *3* (11), 1500389.

52. Low, J.; Jiang, C.; Cheng, B.; Wageh, S.; Al-Ghamdi, A. A.; Yu, J., A Review of Direct Z-Scheme Photocatalysts. *Small Methods* **2017,** *1* (5), 1700080.